Supporting Information

Amyloid Fibril Disruption by Ultrasonic Cavitation: Nonequilibrium Molecular Dynamics Simulations

Hisashi Okumura[*,†,‡] and Satoru G. Itoh[†,‡]

[†]Research Center for Computational Science, Institute for Molecular Science, Okazaki, Aichi 444-8585, Japan

[‡]Department of Structural Molecular Science, The Graduate University for Advanced Studies, Okazaki, Aichi 444-8585, Japan

[*] corresponding author: hokumura@ims.ac.jp

1 Computational Details

The initial conformation was prepared as follows: The model 1 of 2BEG PDB file [1], in which five Aβ(17-42) peptides form intermolecular β-sheet structures between neighboring peptides, was used. The N and C termini of the peptide were capped by acetyl group and N-methyl group, respectively. The amino-acid sequence was Ace-LVFFAEDVGSNKGAIIGLMVGGVVIA-Nme. The five peptides were first minimized by the conjugate gradient method in a vacuum. From the obtained pentamer, two edge peptides were removed. This is because the edge peptides slightly distorted and were not suitable to have intermolecular β-sheet structures with an additional Aβ peptide. Four copies of this trimer were aligned by the rigid translation so that intermolecular β-sheet structures between trimers could be formed. The dodecamer of the Aβ peptides was minimized in a vacuum again, as shown in Fig. 1(a). To discuss the length dependence of the amyloid fibril disruption, we also performed molecular dynamics (MD) simulations of hexamer and trimer systems of the Aβ peptides. The hexamer and trimer of the Aβ peptides were obtained by removing six and nine peptides, respectively from the minimized dodecamer. We put the dodecamer, hexamer, and trimer into a cubic simulation box, the side length of which was $L = 41.47$ Å, with 10168, 11112, and 11591 explicit water molecules, respectively. As counter ions, twelve, six, and three sodium ions were also included in the dodecamer, hexamer, and trimer systems, respectively.

To obtain the initial conditions for the nonequilibrium MD simulations, an equilibrium MD simulation at a fixed volume was first performed for each system for 10 ps at a constant temperature $T = 298$ K. A constant temperature and pressure MD simulation was then performed for 13 ns at $T = 298$ K and at a pressure $P = 0.1$ MPa for equilibration. The four conformations at 10, 11, 12, and 13 ns were employed as the initial conformations for the following nonequilibrium MD simulations for each system. One of the initial conformations of the twelve Aβ peptide system is shown in Fig. 1(b). Starting from the equilibrated conformations, we performed nonequilibrium MD simulations with sinusoidal pressure to mimic the ultrasonic wave. Twenty different initial velocities were used for each system for statistical analysis (five different initial velocities for one initial conformation). Before the nonequilibrium MD simulations, to know at which pressure a bubble was formed within a reasonable simulation time, preliminary MD simulations of the dodecamer system were performed at negative pressure values for 1 ns. Bubble formation was observed at $P = $ -100 MPa, but no bubble was formed at $P = $ -80 MPa. We therefore set the lowest value of the sinusoidal pressure at -100 MPa in the nonequilibrium MD simulations. Time depending pressure was given by

$$P(t) = P_0 + \Delta P \sin(2\pi t/\tau) \tag{1}$$

where $P_0 = 100$ MPa, $\Delta P = 200$ MPa, and $\tau = 1$ ns, as illustrated in Fig. 1(c). Period $\tau = 1$ ns

corresponds to 1 GHz. We performed these nonequilibrium MD simulations for the twelve, six, and three Aβ peptide systems.

We employed the Generalized-Ensemble Molecular Biophysics (GEMB) program developed by H. Okumura [2, 3, 4] to perform the MD simulations. The AMBER parm99SB force field [5] was used for the Aβ peptides and the TIP3P rigid-body model [6] was used for the water molecules. A cubic unit cell was employed with periodic boundary conditions. The electrostatic potential was calculated by the particle mesh Ewald (PME) method [7]. Cutoff distance was $r_\mathrm{c} = 10$ Å for the Lennard-Jone potential. Temperature was controlled at 298 K with the Nosé-Hoover thermostat [8, 9, 10], and pressure was controlled with the Andersen barostat [11]. The symplectic quaternion scheme was used for the rigid-body water molecules [12, 13]. Reversible multiple time step MD techniques [14] were also applied. The time step was taken to be Δt = 0.5 fs for the binding energy of the peptide atoms, $\Delta t = 2.0$ fs for the nonbinding energy of the peptide atoms and that between the peptide atoms and solvent molecules, and $\Delta t = 4.0$ fs for the interaction between the solvent molecules. Because the symplectic rigid-body algorithm was used for the water molecules here, Δt can be taken as long as 4.0 fs [15]. When the bubble collapsed, these time steps should be much shorter. According to instantaneous temperature, time derivative of volume $|\dot{V}/V|$, and instantaneous virial value, the time step was divided into up to 200 short time steps.

The equations of motion to obtain the isobaric-isothermal ensemble for an N atom system at a temperature T and pressure P is given by

$$\dot{\boldsymbol{r}}_i = \frac{\boldsymbol{p}_i}{m_i} + \frac{\dot{V}}{3V}\boldsymbol{r}_i \, , \tag{2}$$

$$\dot{\boldsymbol{p}}_i = \boldsymbol{F}_i - \left(\zeta + \frac{\dot{V}}{3V}\right)\boldsymbol{p}_i \, , \tag{3}$$

$$\dot{\zeta} = \frac{1}{Q}\left(\sum_{i=1}^{N}\frac{\boldsymbol{p}_i^2}{m_i} - gk_\mathrm{B}T\right) \, , \tag{4}$$

$$\dot{V} = \frac{P_V}{M} \, , \tag{5}$$

$$\dot{P}_V = \left\{\frac{1}{3V}\left(\sum_{i=1}^{N}\frac{\boldsymbol{p}_i^2}{m_i} + \sum_{i=1}^{N}\boldsymbol{F}_i \cdot \boldsymbol{r}_i\right) - P\right\} \, , \tag{6}$$

where $\boldsymbol{r}_i$, $\boldsymbol{p}_i$, and m_i is the coordinate, momentum, and mass of atom i, respectively. The vector $\boldsymbol{F}_i$ is the force acting on atom i and P_V is the momentum for volume V. The variable ζ is a degree of freedom for the Nosé-Hoover thermostat. The constant Q and M are the artificial "mass" associated with the thermostat and barostat, respectively. The constant g is the number of degrees of freedom. In the case of the system consisting of N atoms, g is equal to $3N$. The dot () stands for the real-time derivative d/dt. The equations of motion for rigid-body molecules in the isobaric-isothermal ensemble are given in Ref. [15].

In the calculation of the physical quantities for hydrophilic and hydrophobic residues, Glu, Asp, Ser, Asn, and Lys were regarded as hydrophilic and Leu, Val, Phe, Ala, Ile, and Met were regarded as hydrophobic. Gly was included in neither hydrophilic nor hydrophobic residues. The hydration water molecule was defined here as a water molecule, the oxygen atom of which is within 5 Å from any protein heavy atoms, i.e. carbon, oxygen, nitrogen, and sulfur atoms.

The bubble volume V_{bub} was calculated as follows. The time series of the volume of the whole system was almost the same in each period of set pressure, except for when the bubble was formed. Thus, an average of the volume was taken over twenty initial conditions and the periods when the bubble was not formed. We then define the bubble volume V_{bub} as the difference between the volume when the bubble was formed and this average volume.

One might doubt the accuracy of PME when a bubble was formed and the system size was large, because the grid size for fast Fourier transform in PME is typically 1 Å. To clarify this, we calculated electrostatic potential energy E_{elec} at the largest system size ($t = 1.006$ ns) in Fig. 3 by both PME and original Ewald methods. The results were $E_{\mathrm{elec}} = -0.91530246 \times 10^5$ kcal/mol by the PME method and $E_{\mathrm{elec}} = -0.91530175 \times 10^5$ kcal/mol by the Ewald method. The difference was only 0.000078 % and negligible. This is because the real-space and self parts of the electrostatic potential energy are dominant and much larger than the reciprocal-space part in our simulations.

2   Results and discussion

The time series of the number of hydration water molecules per residue $N_{\mathrm{H_2O}}/N_{\mathrm{residue}}$, the fraction of nonhydrated residues $f_{\mathrm{nonhydrated}}$, the fraction of β-sheet f_β, bubble volume V_{bub}, and pressure are presented in Figs. S1-S3. In most of the simulations of the dodecamer and hexamer of the Aβ peptides, a bubble was formed around the hydrophobic residues in the transmembrane (TM) region. Most β-strands maintained their secondary structures in the bubble. When the bubble collapsed, $N_{\mathrm{H_2O}}/N_{\mathrm{residue}}$ of the hydrophilic and hydrophobic residues in the nontransmembrane (NTM) region had a sharp peak because the water molecules crashed against the hydrophilic residues in the NTM region. The amyloid fibrils were then disrupted. Only in the MD simulation of the dodecamer from initial condition 8, other bubble formation was observed at the seventh negative pressure, as shown in Fig. S1(H). However, except in this trajectory, no bubble was formed again after the amyloid fibril was disrupted.

The time series of $N_{\mathrm{H_2O}}/N_{\mathrm{residue}}$, $f_{\mathrm{nonhydrated}}$, and V_{bub} before and after bubble formation are presented in Figs. S4-S6. Before the bubble was formed, small bubbles or cavities were formed and collapsed for several times in all MD simulations of the dodecamer and hexamer systems. In most cases, the cavity size in the second section ($P < -75$ MPa, green lines)

was larger than the first section ($P > -75$ MPa, blue lines). In the trimer system, bubble formation was observed only in one MD trajectory (Figs. S3(Q) and S6(Q)). Even if a bubble was not formed, fluctuation of V_{bub} was also larger at high and negative pressure than at low and negative pressure.

As stated in the main text, bubble formation depends on the magnitude and period of negative pressure. A bubble is easily formed under high and long-term negative pressure. Actually, when we performed simulations under constant negative pressure values, it took around 100 ps at -100 MPa and around 500 ps at -90 MPa for bubble formation, while no bubble formation was observed during 1 ns at -80 MPa. To check the robustness of the trends in the amyloid fibril length (Fig. 5 in the main text) to variation in reference pressure ($P_0 = 100$ MPa) and frequency ($f = 1.0$ GHz), we ran other sets of MD simulations at different parameter values. Here, we employed three sets of the parameters: ($P_0 = 50$ MPa, $f = 1.0$ GHz), ($P_0 = 100$ MPa, $f = 0.5$ GHz), and ($P_0 = 50$ MPa, $f = 0.5$ GHz). The minimum pressure value $P_{\min} = -100$ MPa was fixed, that is, $\Delta P = 150$ MPa for $P_0 = 50$ MPa and $\Delta P = 200$ MPa for $P_0 = 100$ MPa, as shown in Fig. S7. The results are shown in Fig. S8. We observed the same trends at all sets of conditions of frequency and pressure. These results support our conclusions that disruption of shorter amyloids required more time of negative pressure and are consistent with the experiments in which the length of the amyloid fibril were almost the same by ultrasonication. We can also see that as the frequency decreased, the amyloid fibrils were disrupted with less occurrences of negative pressure. This is because the period of negative pressure increased and a bubble was formed with higher probability as the frequency decreased, as illustrated in Fig. S7. We note that the ratio of the period of negative pressure to that of positive pressure increases as P_0 decreases with the fixed $P_{\min}$, as illustrated in Fig. S9. If this ratio increases, the set pressure may become negative again before the bubble collapses. If $P_{\min}$ increases to zero and P_0 decreases with this ratio fixed to, for example, the values in our simulation, the set pressure does not become negative before the bubble collapses. This is why we set P_0 as 100 MPa and 50 MPa.

The fact that the water molecules crashed against the hydrophilic residues in the NTM region means that the dipole moments of the water molecules were interacting with the charges and dipole moments of the hydrophilic residues. In the bubble formation and collapse, liquid-gas phase transition occurs. When water goes from liquid to gas phase, the average dipole moment of a water molecule decreases from 2.6 D to 1.8 D. Because water crashed against the amyloid fibril as a droplet, the dipole moment on the surface should decrease not to 1.8 D but 2.0 D [16]. We used the TIP3P force field for the water molecules here. To include the effect of the dipole moment decrease in the future, it is preferred to employ a polarizable force filed, such as AMOEBA [17] and Thole model [18] instead of a nonpolarizable force filed such as

TIP3P. However, the qualitative trend that the water molecules crash against the NTM region of the amyloid fibril should be unchanged because the water molecule still has a dipole moment even on the droplet surface.
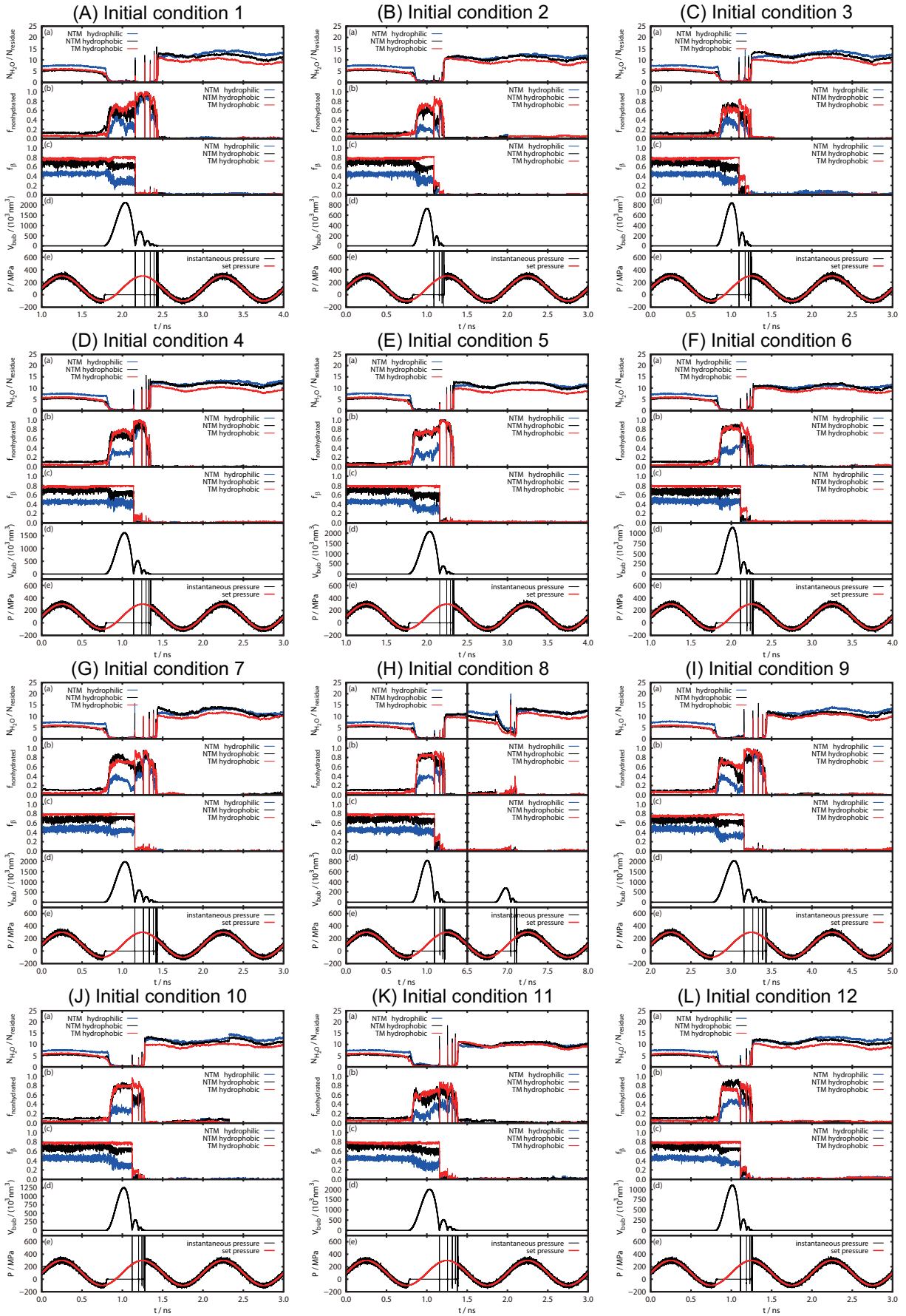
Figure S1: Time series obtained from twenty MD simulations of the dodecamer of the Aβ peptides. See the caption of Fig. 3 for details.
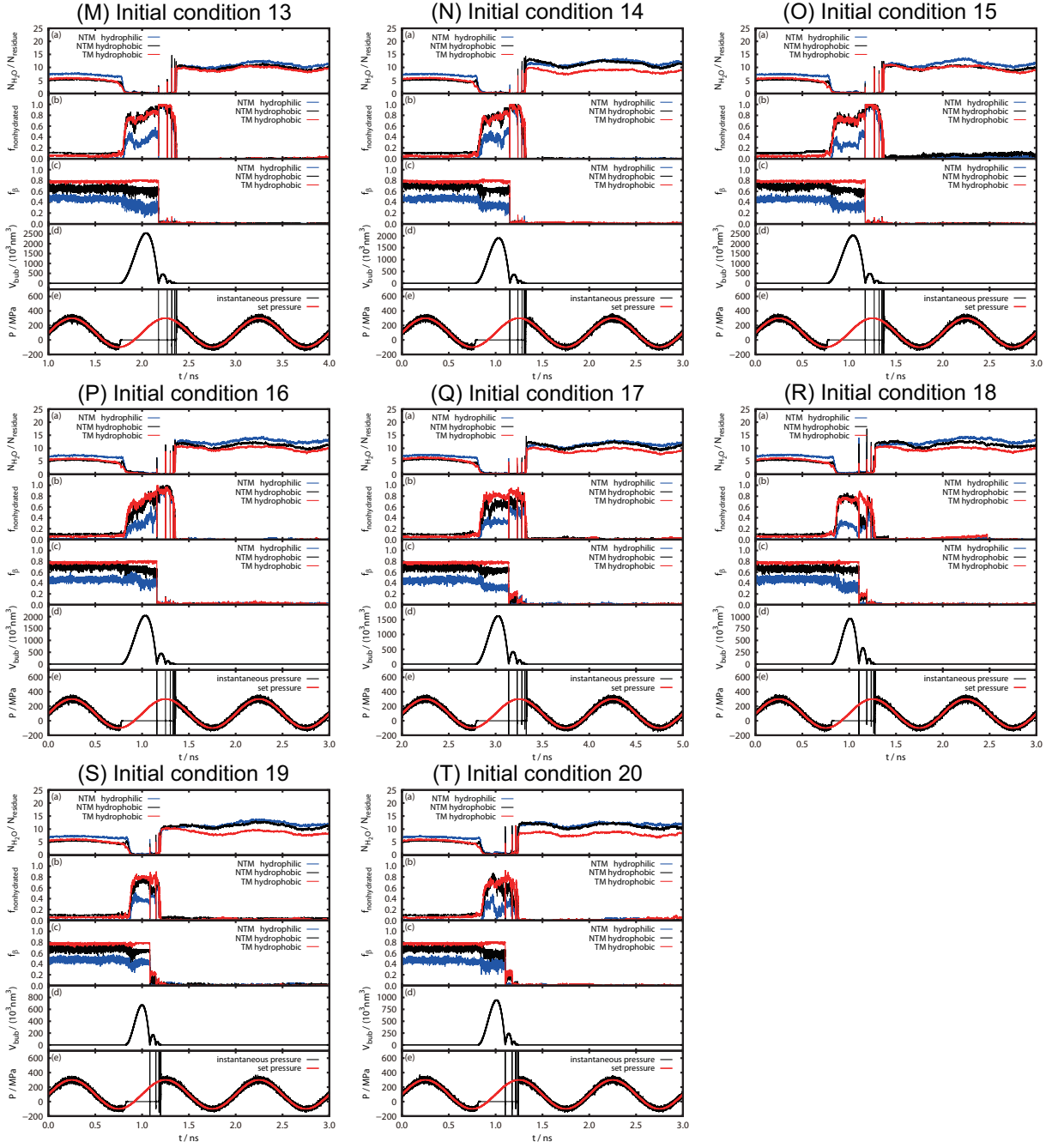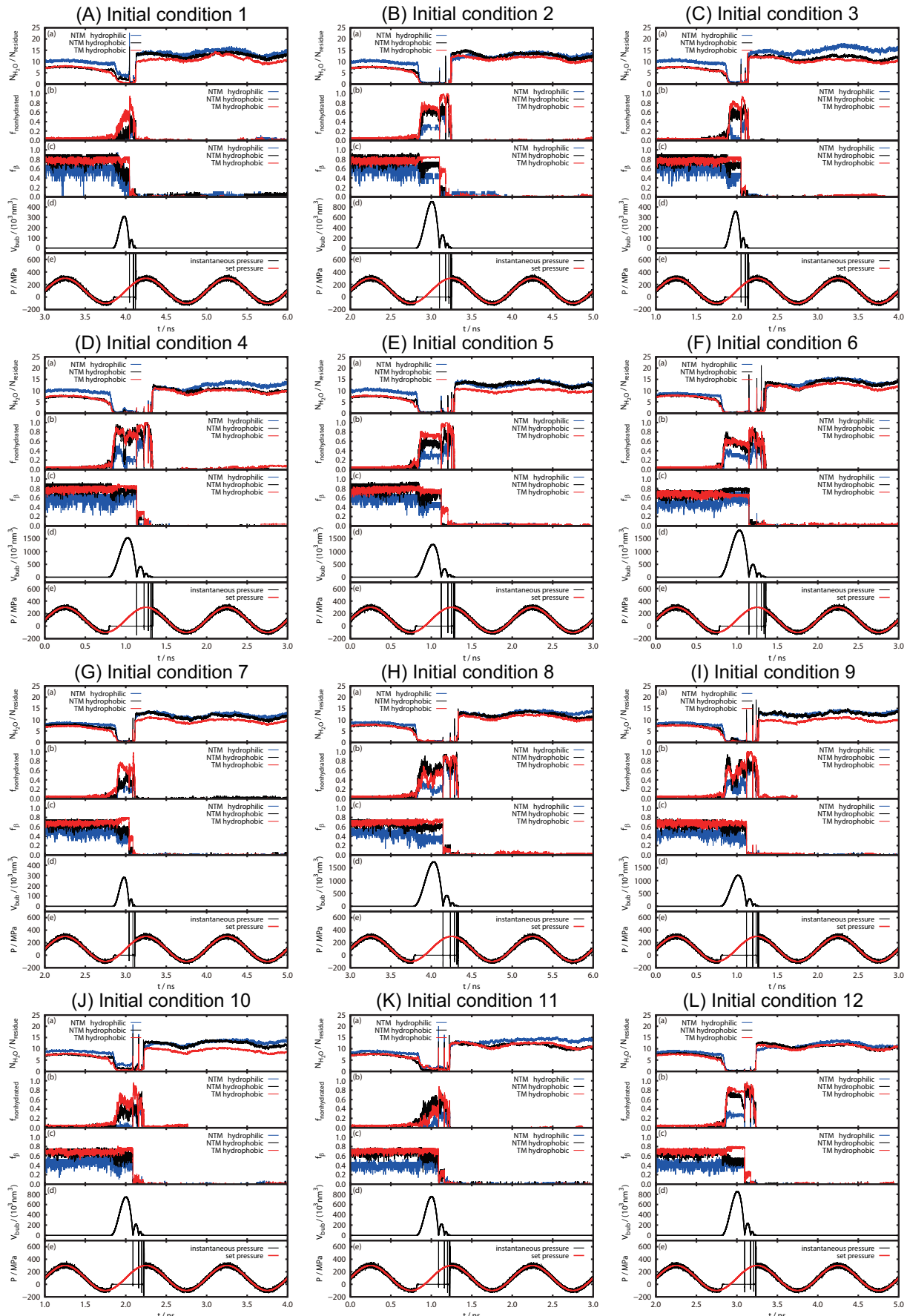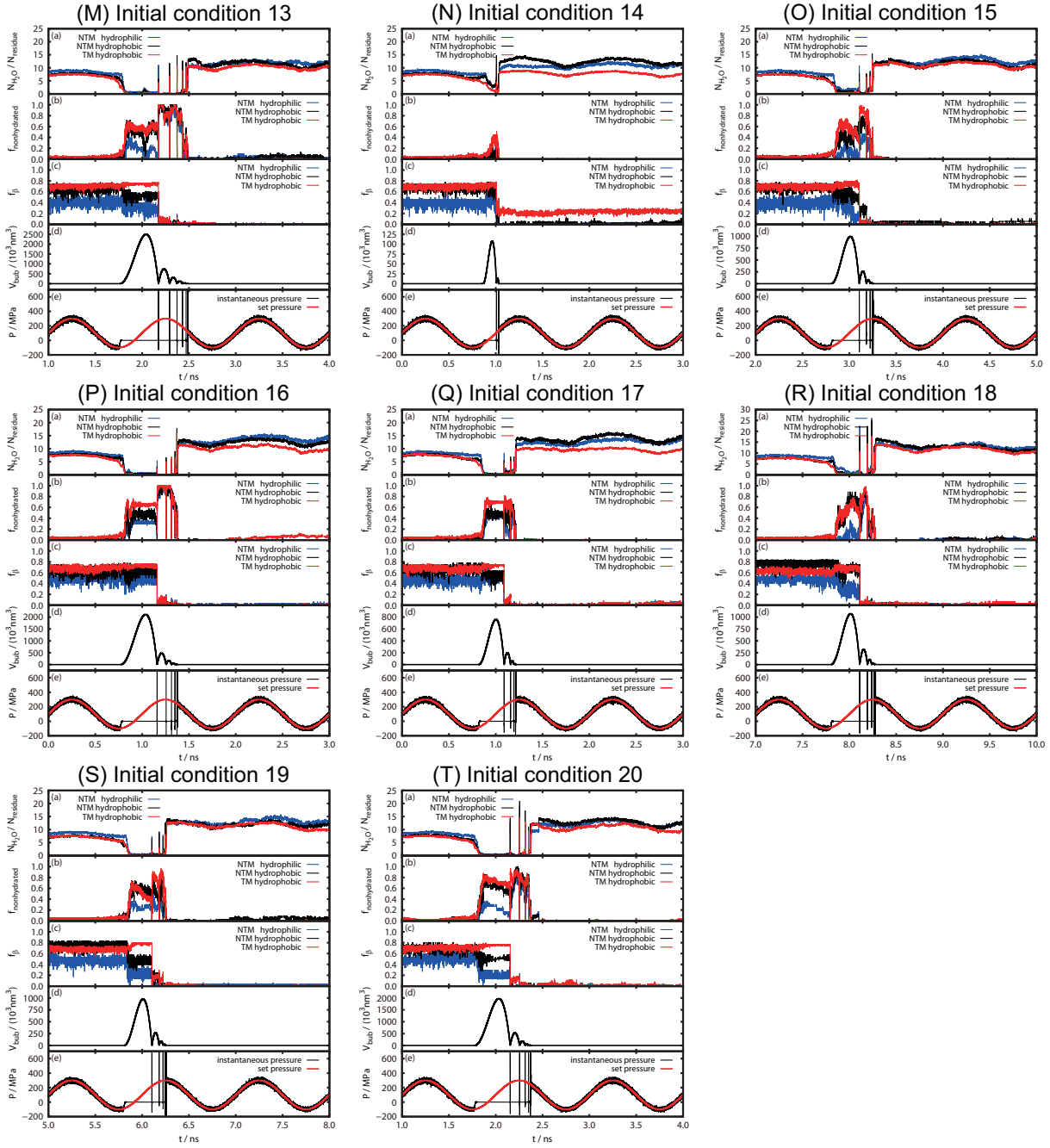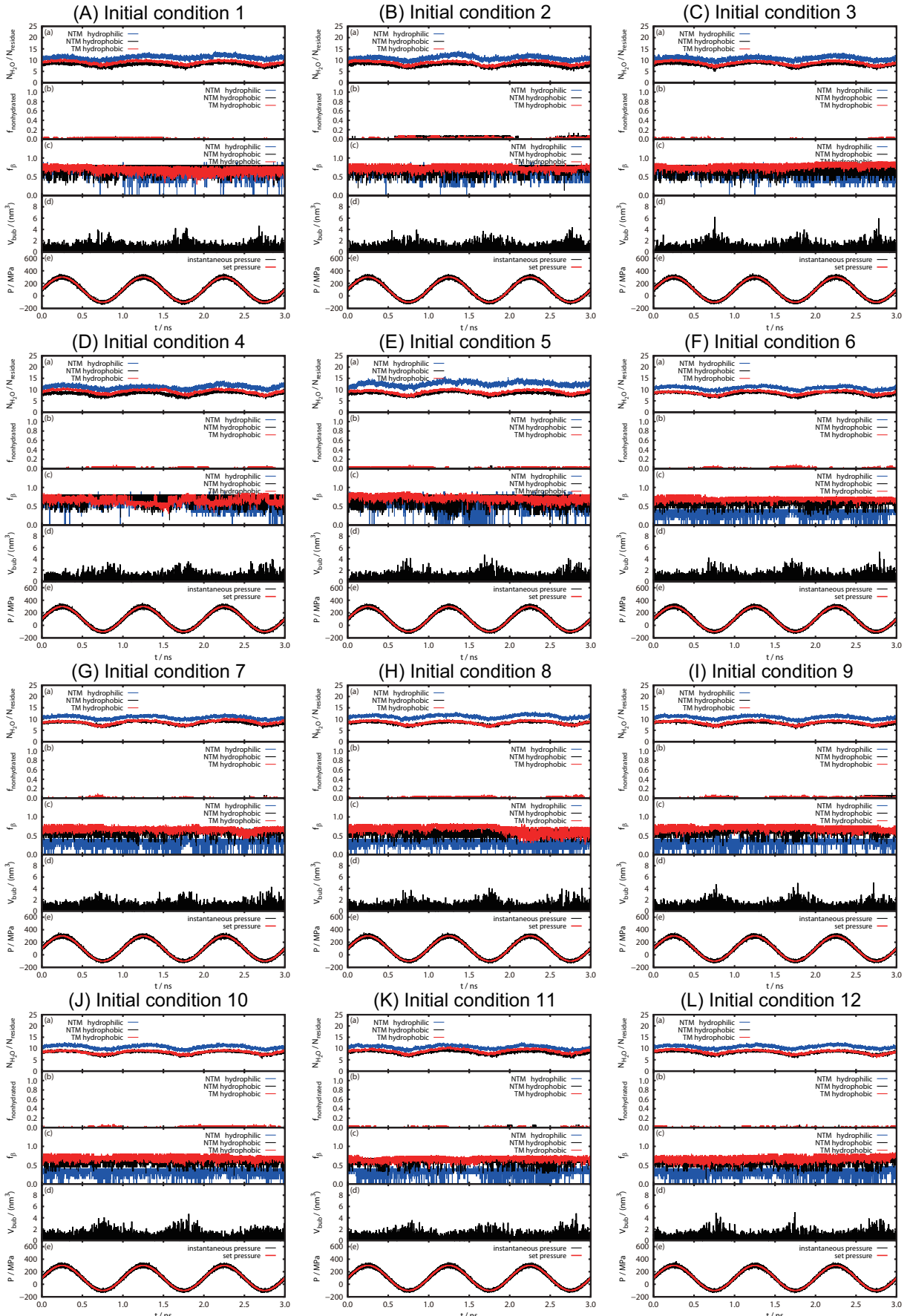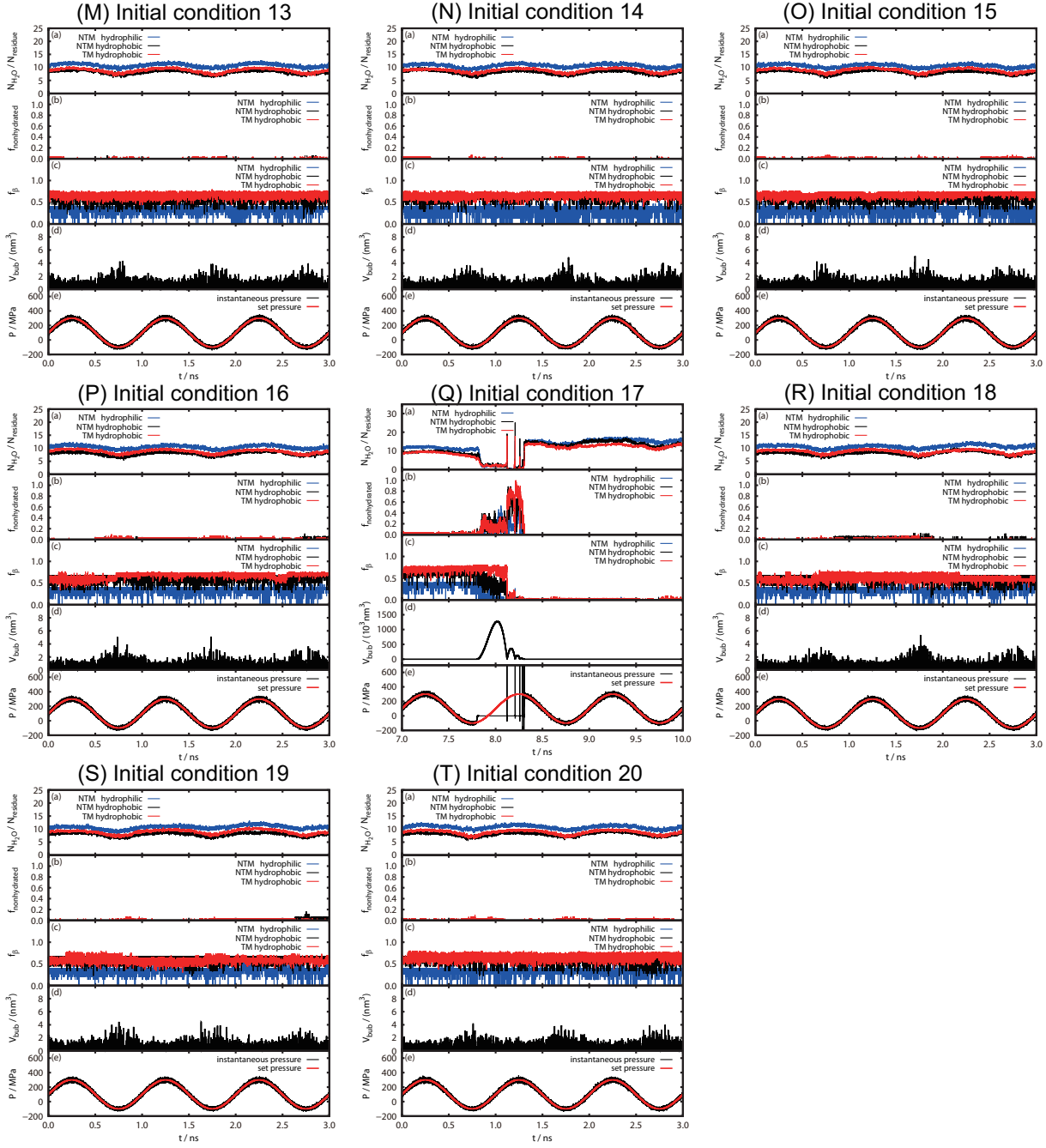
Figure S1(continued): Time series obtained from twenty MD simulations of the dodecamer of the Aβ peptides. See the caption of Fig. 3 for details.
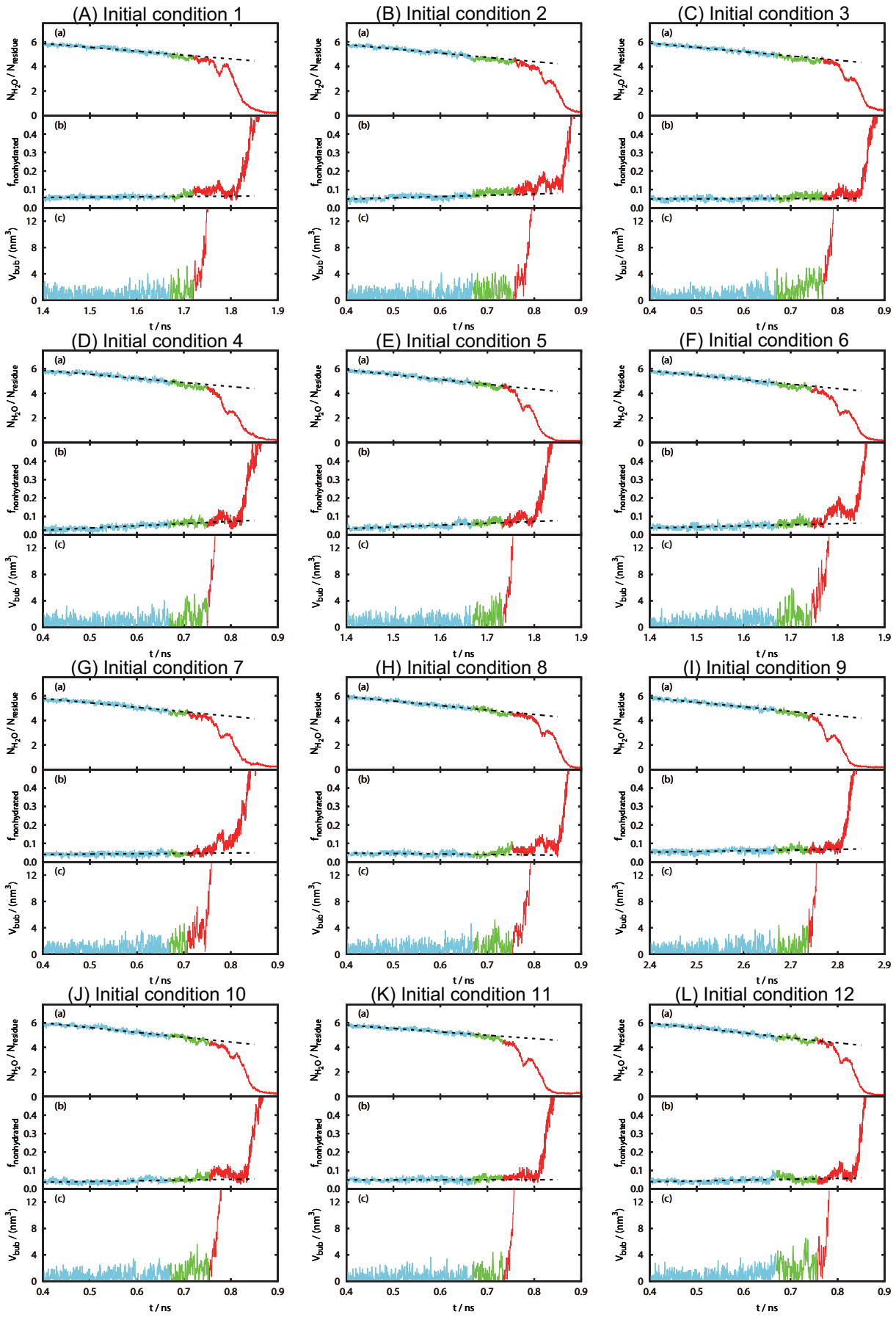
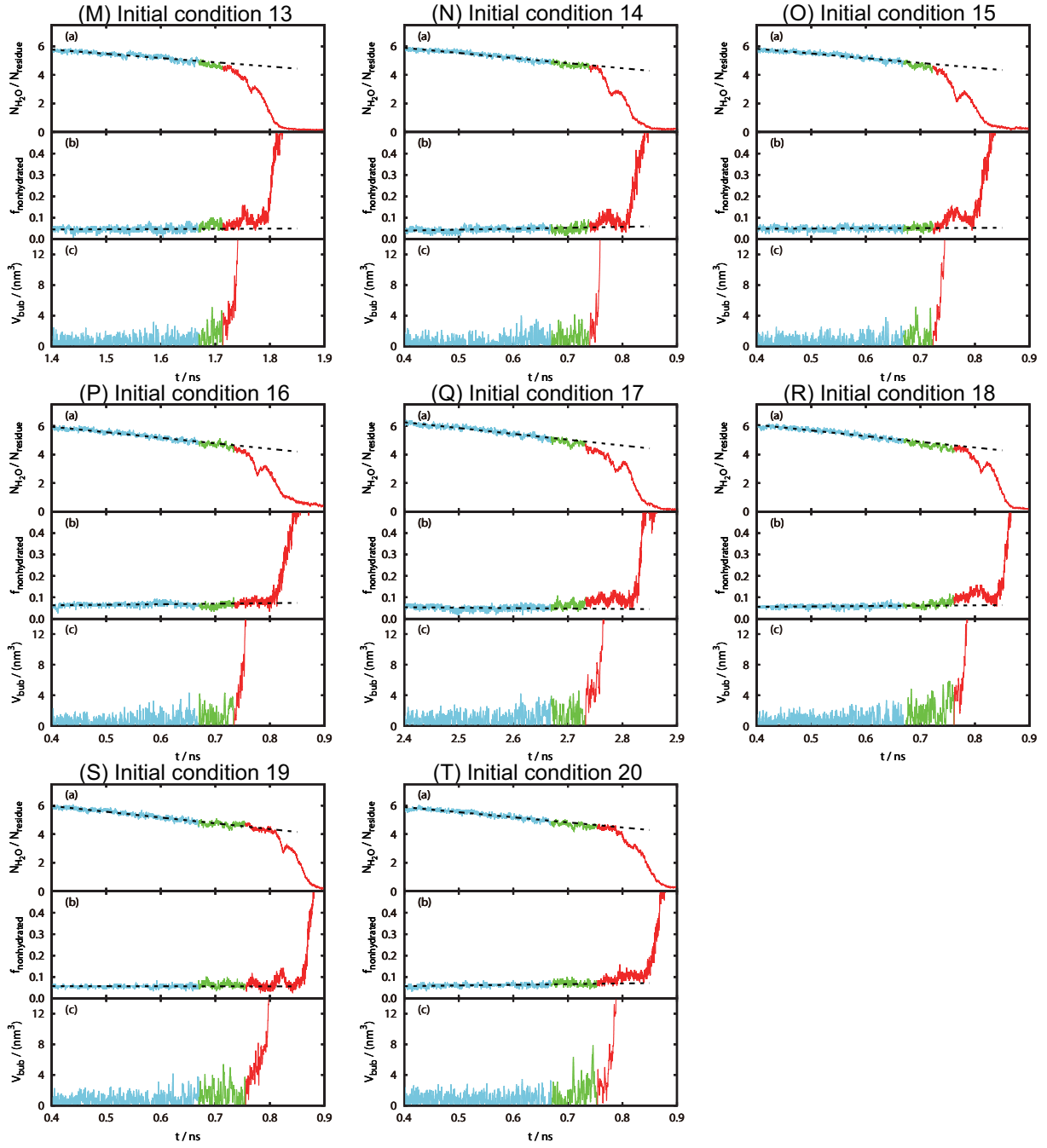Figure S2: Time series obtained from twenty MD simulations of the hexamer of the Aβ peptides. See the caption of Fig. 3 for details.

Figure S2(continued): Time series obtained from twenty MD simulations of the hexamer of the Aβ peptides. See the caption of Fig. 3 for details.

Figure S3: Time series obtained from twenty MD simulations of the trimer of the Aβ peptides. See the caption of Fig. 3 for details.

Figure S3(continued): Time series obtained from twenty MD simulations of the trimer of the Aβ peptides. See the caption of Fig. 3 for details.

Figure S4: Time series before and after bubble formation obtained from twenty MD simulations of the dodecamer of the Aβ peptides. See the caption of Fig. 4 for details.
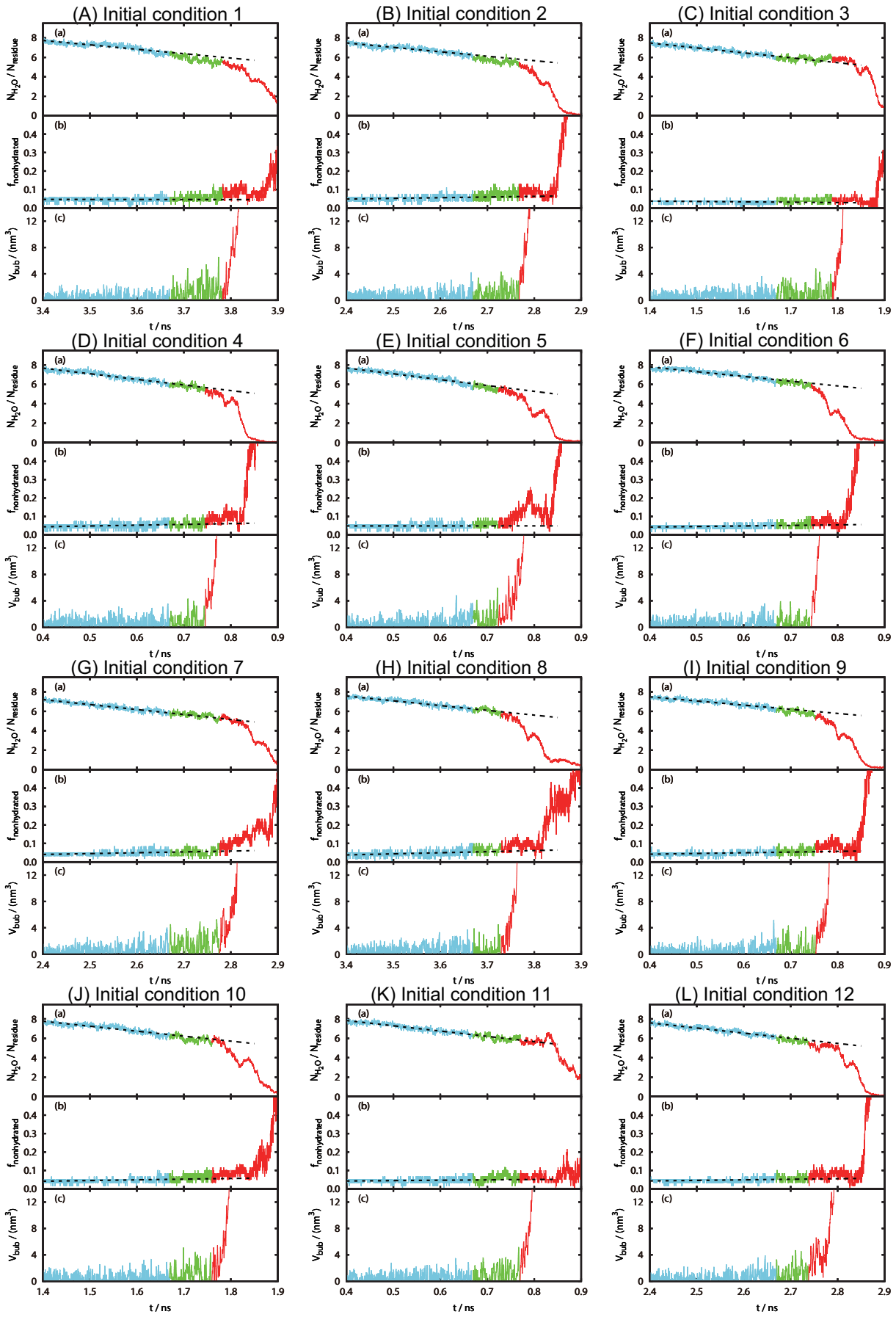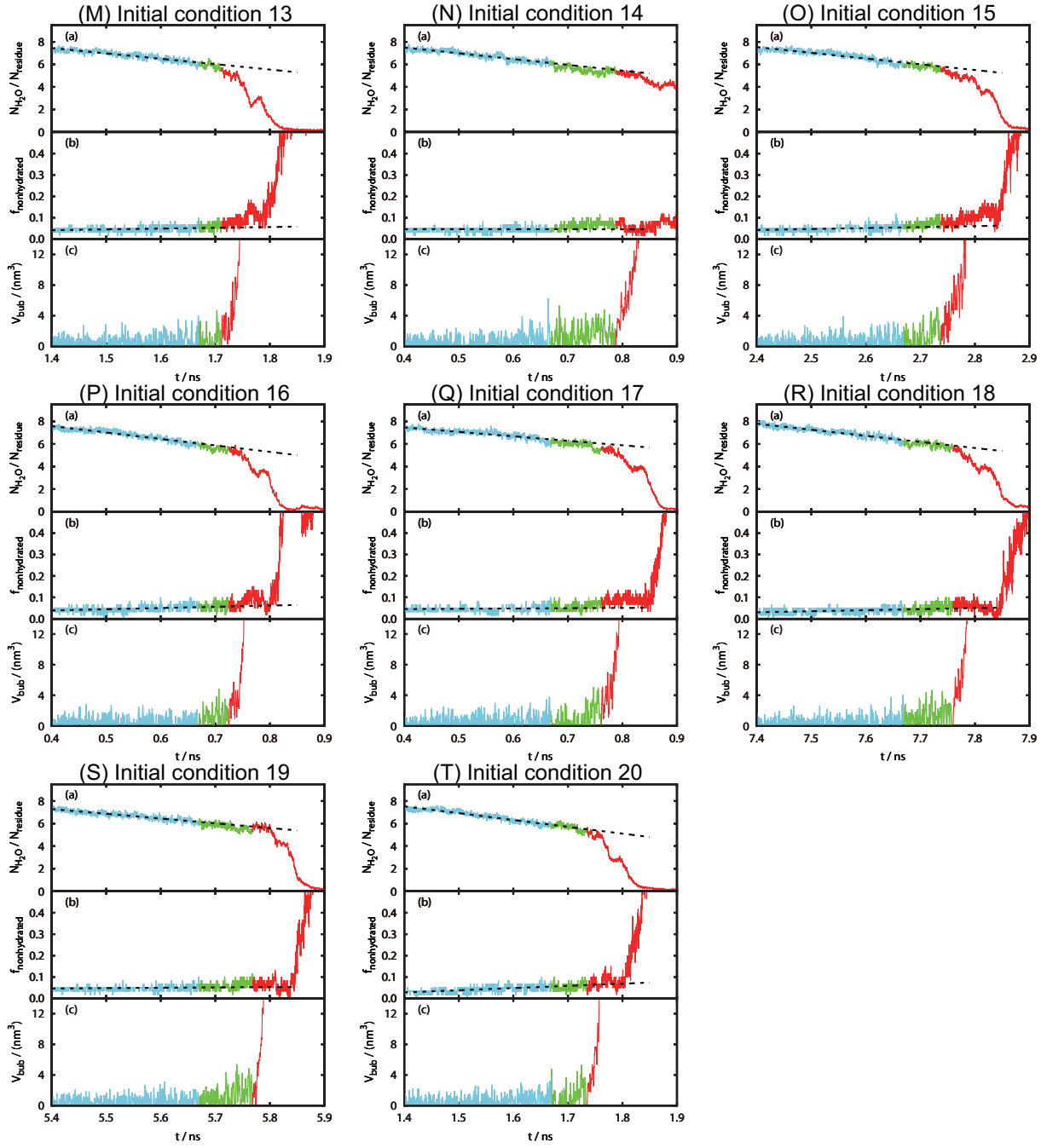
Figure S4(continued): Time series before and after bubble formation obtained from twenty MD simulations of the dodecamer of the Aβ peptides. See the caption of Fig. 4 for details.

Figure S5: Time series before and after bubble formation obtained from twenty MD simulations of the hexamer of the Aβ peptides. See the caption of Fig. 4 for details.
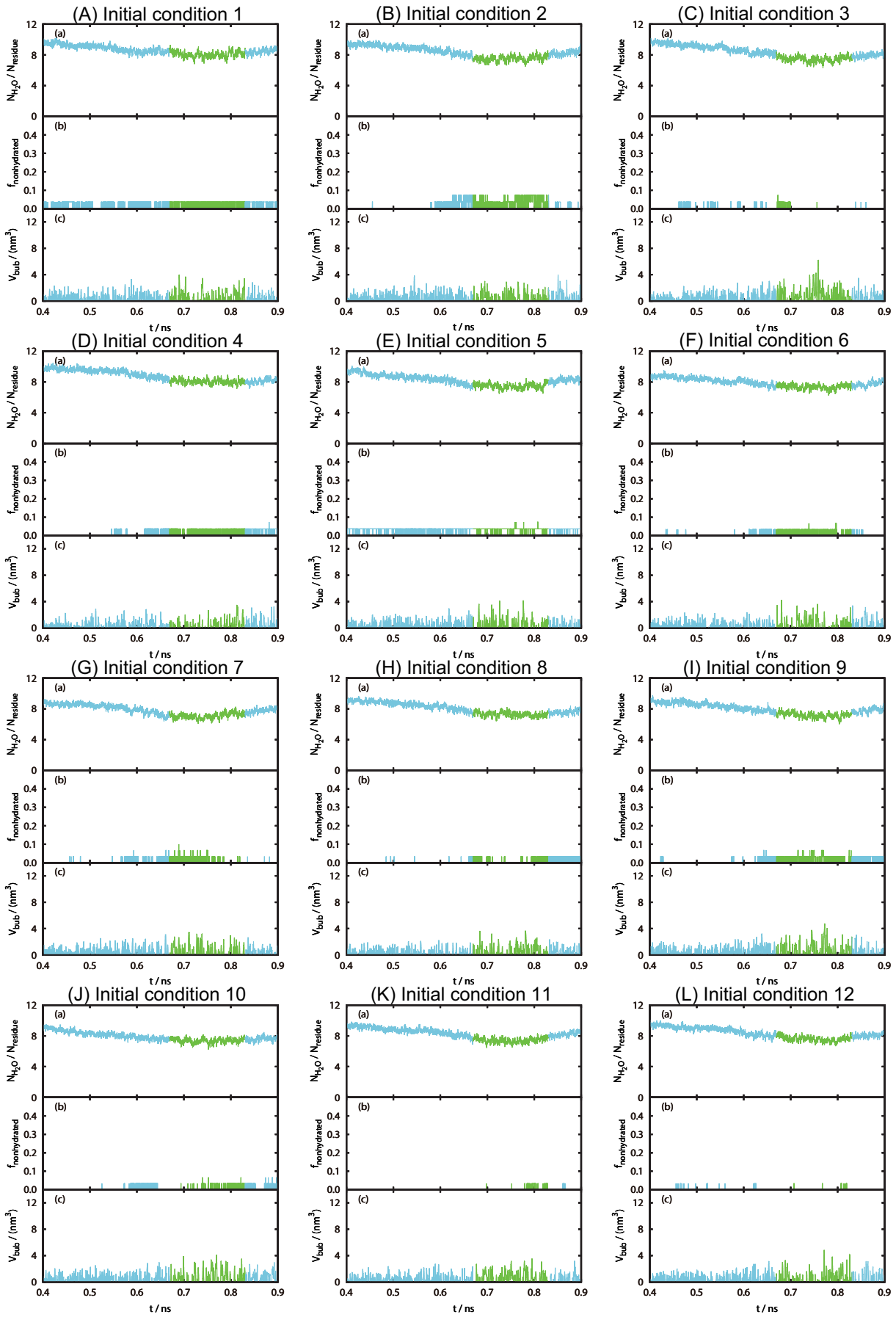
S15

Figure S5(continued): Time series before and after bubble formation obtained from twenty MD simulations of the hexamer of the Aβ peptides. See the caption of Fig. 4 for details.

Figure S6: Time series before and after the highest negative pressure obtained from twenty MD simulations of the trimer of the Aβ peptides. See the caption of Fig. 4 for details.
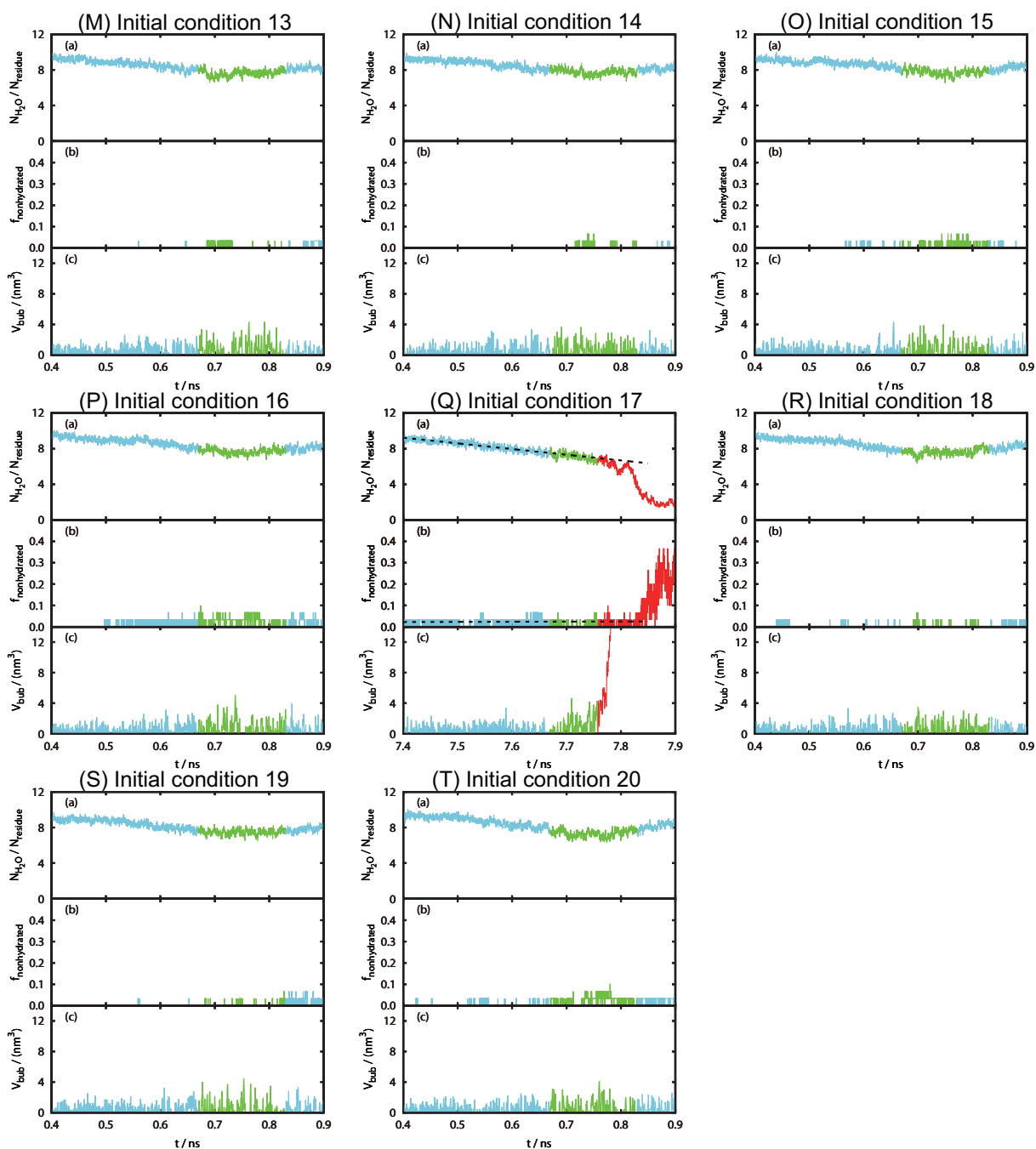
Figure S6(continued): Time series before and after the highest negative pressure obtained from twenty MD simulations of the trimer of the Aβ peptides. See the caption of Fig. 4 for details.
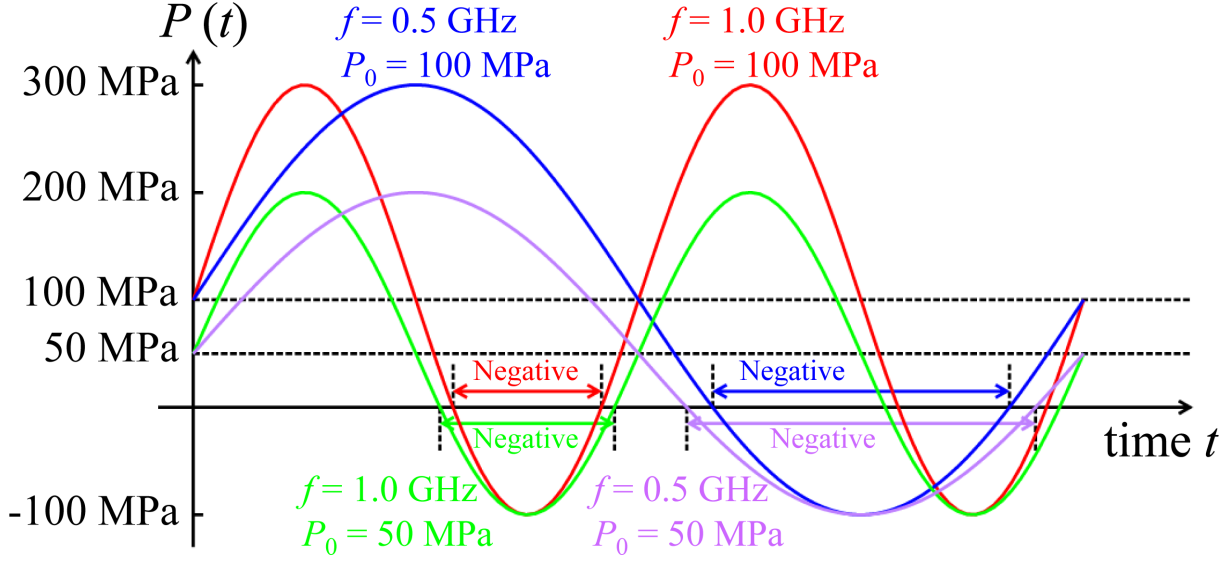
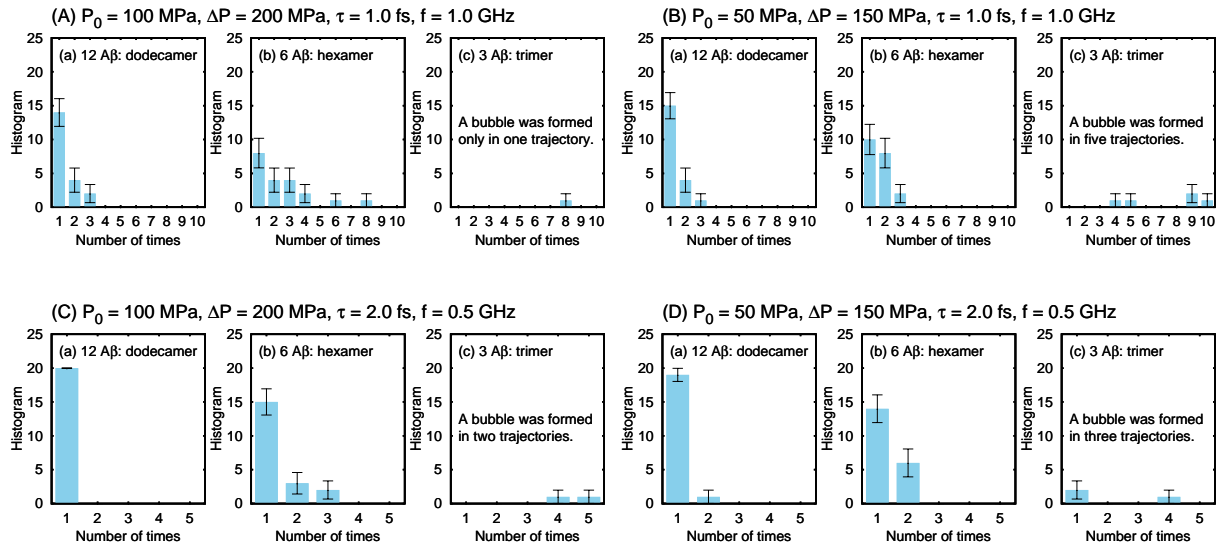Figure S7: Sinusoidal evolution of the set pressure as a function of time employed in the MD simulations.

Figure S8: Histograms showing how many times pressure had been negative before bubbles were formed at four sets of sinusoidal pressure parameters. See the caption of Fig. 5 for details.
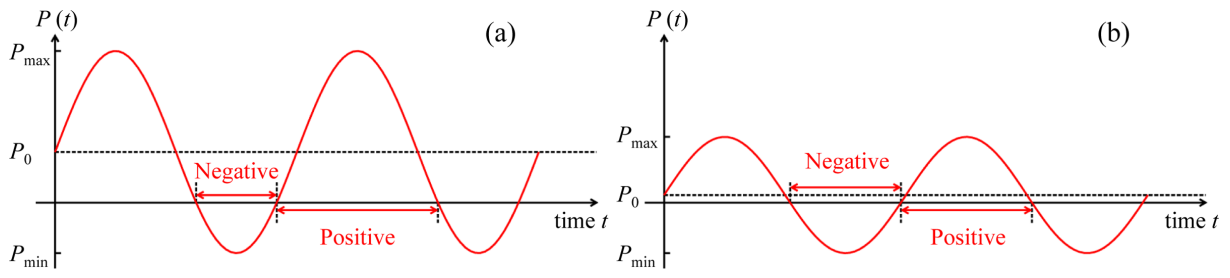
Figure S9: Sinusoidal evolution of the set pressure as a function of time at fixed (a) high P_0 and (b) low P_0 with $P_{\min}$.

References

[1] Luhrs, T.; Ritter, C.; Adrian, M.; Riek-Loher, D.; Bohrmann, B.; Dobeli, H.; Schubert, D.; Riek, R. *Proc. Natl. Acad. Sci. USA* **2005**, 102, 17342-17347.

[2] Okumura, H.; Okamoto, Y. *J. Phys. Chem. B* **2008**, 112, 12038-12049.

[3] Okumura, H. *Proteins* **2012**, 80, 2397-2416.

[4] Okumura, H.; Itoh, S. G. *Phys. Chem. Chem. Phys.* **2013**, 15, 13852-13861.

[5] Hornak, V.; Abel, R.; Okur, A.; Strockbine, B.; Roitberg, A.; Simmerling, C. *Proteins* **2006**, 65, 712-725.

[6] Jorgensen, W. L.; Chandrasekhar, J.; Madura, J. D.; Impey, R. W.; Klein, M. L. *J. Chem. Phys.* **1983**, 79, 926-925.

[7] Essmann, U.; Perera, L.; Berkowitz, M. L.; Darden, T.; Lee, H.; Pedersen, L. G. *J. Chem. Phys.* **1995**, 103, 8577-8593.

[8] Nosé, S. *Mol. Phys.* **1984**, 52, 255-268.

[9] Nosé, S. *J. Chem. Phys.* **1984**, 81, 511-519.

[10] Hoover, W. G. *Phys. Rev. A* **1985**, 31, 1695-1697.

[11] Andersen, H. C. *J. Chem. Phys.* **1980**, 72, 2384-2393.

[12] Yoshida, H. *Phys. Lett. A* **1990**, 150, 262-268.

[13] Miller, T. F.; Eleftheriou, M.; Pattnaik, P.; Ndirango, A.; Newns, D.; Martyna, G. J. *J. Chem. Phys.* **2002**, 116, 8649-8659.

[14] Tuckerman, M.; Berne, B. J.; Martyna, G. J. *J. Chem. Phys.* **1992**, 97, 1990-2001.

[15] Okumura, H.; Itoh, S. G.; Okamoto, Y. *J. Chem. Phys.* **2007**, 126, 084103.

[16] Chang, T.-M.; Dang, L. X. *Chem. Rev.* **2006**, 106, 1305-1322.

[17] Ren, P; Ponder, J. W. *J. Phys. Chem.* **2003**, 107, 5933-5947.

[18] Thole, R. T. *Chem. Phys.* **1981**, 59, 341-350.